Research Article | Vol. 26, No. 8 | 16 Apr 2018 | OPTICS EXPRESS 11034
Optics EXPRESS

MTF measurements of a type-II superlattice infrared focal plane array sealed in a cryocooler

JEAN NGHIEM,[1,*] JULIEN JAECK,[1] JEROME PRIMOT,[1] CHRISTOPHE COUDRAIN,[1] SOPHIE DERELLE,[1] EDOUARD HUARD,[1] MARCEL CAES,[1] SYLVIE BERNHARDT,[1] RIAD HAIDAR,[1] PHILIPPE CHRISTOL,[2] AND ISABELLE RIBET-MOHAMED[1]

[1] *ONERA, Chemin de la Hunière, F- 91761 Palaiseau, France*
[2] *IES, Univ. Montpellier, CNRS, F-34000 Montpellier, France*
[*] *isabelle.ribet@onera.fr*

Abstract: In operational electro-optical systems, infrared focal plane arrays (IR FPA) are integrated in cryocoolers which induce vibrations that may strongly affect their modulation transfer function (MTF). In this paper, we present the MTF measurement of an IR FPA sealed in its cryocooler. The method we use to measure the MTF decorrelates operational constraints and the technological limitations of the IR FPA. The bench is based on the diffraction properties of a continuously self imaging grating (CSIG). The 26 μm pixel size extracted from the MTF measurement is in good agreement with the expected value.

OCIS codes: (040.0040) Detectors; (040.1240) Arrays; (040.3060) Infrared; (110.4100) Modulation transfer function; (070.6760) Talbot and self-imaging effects.

References and links

1. M. Razeghi, A. Haddadi, A. M. Hoang, G. Chen, S. Bogdanov, S. R. Darvish, F. Callewaert, P. R. Bijjam, and R. McClintock, "Antimonide-Based Type II Superlattices: A Superior Candidate for the Third Generation of Infrared Imaging Systems," J. Electron. Mater. **43**, 2802–2807 (2014).
2. E. Giard, I. Ribet-Mohamed, J. Jaeck, T. Viale, R. Haïdar, R. Taalat, M. Delmas, J.-B. Rodriguez, E. Steveler, N. Bardou, F. Boulard, and P. Christol, "Quantum efficiency investigations of type-II InAs/GaSb midwave infrared superlattice photodetectors," J. Appl. Phys. **116**(4) 043101 (2014).
3. R. Rehm, M. Walther, J. Schmitz, F. Rutz, J. Fleißner, R. Scheibner, and J. Ziegler, "InAs/GaSb superlattices for advanced infrared focal plane arrays," Infrared Phys. Technol. **52**(6), 344–347 (2009).
4. M. Delmas, J.-B. Rodriguez, R. Rossignol, A. S. Licht, E. Giard, I. Ribet-Mohamed, and P. Christol, "Identification of a limiting mechanism in GaSb-rich superlattice midwave infrared detector," J. Appl. Phys. **119**(117), 174503 (2016).
5. M. Delmas, R. Rossignol, J. B. Rodriguez, and P. Christol, "Design of InAs/GaSb superlattice infrared barrier detectors," Superlattice. Microstruct. **104**, 402-414 (2017).
6. L. Höglund, C. Asplund, R. Marcks von Würtemberg, H.Kataria, A. Gamfeldt, S. Smuk, H. Martijn, and E. Costard, " Manufacturability of type-II InAs/GaSb superlattice detectors for infrared imaging," Infrared Phys. Technol. **84**(6), 28–32 (2017).
7. P. C. Klipstein, Y. Livneh, A. Glozman, S. Grossman, O. Klin, N. Snapi, and E. Weiss, "Modeling InAs/GaSb and InAs/InAsSb Superlattice Infrared Detectors," J. Electron. Mater. **43**(8), 2984–2990 (2014).
8. A. Rogalski, "Recent progress in infrared detector technologies," Infrared Phys. Technol. **54**, 136–154 (2011).
9. N. Guérineau, and J. Primot, "Nondiffracting array generation using an N-wave interferometer," J. Opt. Soc. Am. A **16**, 293-298 (1999).
10. F. de la Barrière, G. Druart, N. Guérineau, S. Rommeluère, L. Mugnier, O. Gravrand, N. Baier, N. Lhermet, G. Destefanis, and S. Derelle, "Modulation transfer function measurement of infrared focal-plane arrays with small fill factors," J. Electron. Mater. **41**(10) 2730–2737 (2012).
11. N. Guérineau, B. Harchaoui, J. Primot, and K. Heggarty, "Generation of achromatic and propagation-invariant spot arrays by use of continuously self-imaging gratings," Opt. Lett. **26**, 411–413 (2001).
12. E. Di Mambro, N. Guérineau, and J. Primot, "Modulation transfer function measurement of an infrared focal plane array using a continuously self-imaging grating," Proc.SPIE **5076**, 169–178 (2003).
13. J. E. Greivenkamp, and A. E. Lowman, "Modulation transfer function measurement of sparse-array sensors using a self-calibrating fringe pattern," Appl. Opt. **33**(22), 5029–5036 (1994).
14. G. Druart, S. Rommeluère, T. Viale, N. Guérineau, I. Ribet-Mohamed, A. Crastes, A. Durand, and J. Taboury, "Modulation transfer function measurement of microbolometer focal plane array by Lloyd ´s mirror method," Proc. SPIE **9071**, 90710S (2014).

#319121 https://doi.org/10.1364/OE.26.011034
Journal © 2018 Received 11 Jan 2018; revised 20 Mar 2018; accepted 21 Mar 2018; published 13 Apr 2018

Optics EXPRESS

15. G. Boreman, and E. L. Dereniak, "Method for measuring modulation transfer function of charge-coupled devices using laser speckle," Opt. Eng. **25**(1), 148 (1986).
16. A. Daniels, G.D. Boreman, A. D. Ducharme, and E. Sapir, "Random transparency targets for modulation transfer function measurement in the visible and infrared regions," J. Opt. Soc. Am. B **34**(3), 860–868 (1995).
17. M. Piponnier, G. Druart, N. Guérineau, J. -L. de Bougrenet, and J. Primot, "Optimal conditions for using the binary approximation of continuously self-imaging gratings," Opt. Express **19**(23) 23054–23066 (2011).
18. J. Primot, G. Rousset, and J. C. Fontanella, "Deconvolution from wave-front sensing: a new technique for compensating turbulence-degraded images," J. Opt. Soc. Am. A **7**, 1598-1608 (1990).

1. Introduction

The modulation transfer function (MTF) of a detector is a very sought after figure of merit (FoM) by technologists and system designers alike. It provides the former valuable feedbacks on the quality of the process (etching steepness or depth for instance) and intrinsic properties of the material such as electronic diffusion length; the latter will harness the MTF to modelize pixel filtering and compare it to the optical filtering, in order to optimize the system overall performance.

There are quite many challenges when attempting to measure a detector MTF in the infrared domain (IR). First, the trend of smaller pixels means the diffraction limit and deconvolution become major concerns. As a result, constraints are harsher on any projection optics used in measurement benches. They have to reconcile low chromatism and high aperture while operating within a relatively large spectral band. Such attributes are difficult to achieve at the same time and likely come at a prohibitive cost. Spectral filters and reduced aperture can be used to lower the requirements on optics in the measurement bench but the Signal to Noise Ratio (SNR) is lowered as well. Second, the fact that most high performance IR technologies are cooled limits the physical access to the focal plane array (FPA). Alignment and focalization are then more delicate in the setup. Third, another issue to address is that operational IR focal plane arrays are often packaged as Integrated Detector Dewar Cooler Assembly (IDDCA), so the f-number is set by the cold shield. Moreover, IDDCA configuration implies the use of a cryocooler that introduces vibrations on the FPA. It translates into motion blur that affects the detector MTF one wants to measure. These vibrations have to be dampened or taken into account when attempting to measure the detector MTF. Our solution to address the three aforementioned issues is a MTF measurement bench exploiting the self-imaging panchromatic property of achromatic gratings to project a high resolution periodic pattern on the FPA. It requires neither high quality projection optics nor demanding alignments for the detector MTF to be measured.

The type-II superlattice (T2SL) FPA has been chosen to illustrate our MTF measurement technique since no such characterization has been made so far on the T2SL technology integrated in a cryocooler, that is to say in an operational packaging. Indeed T2SL have shown promising prospects thus far [1–8]. Thus, it is a suitable candidate for high performance infrared imaging applications in which the MTF measurement is demanded.

In this paper we present the MTF measurements of a 30 µm pitch 320x256 MWIR type-II superlattice infrared Focal Plane Array sealed in a cryocooler. We first present the bench principle and how it is designed.The second part of this paper is dedicated to the vibration study, as they can strongly affect the MTF. The use of accelerometers combined with low integration time measurements allows to distinguish the vibration effect from other contributions on the measured MTF.

2. Experimental setup

2.1. Principle of measurement

The keystone of the bench presented in this paper is the Continuously Self Imaging Grating (CSIG). The CSIG diffracts a set number N of orders (usually CSIGs are engineered to diffract 12, 24 or

48 orders). The fact that these orders are designed to be localized on the Montgomery circle [9] grants the achromatic and propagation-invariant property to the projected pattern [10–12]. It completely deletes the need of projection optics (and their constraints along) and neither alignment nor focusing distance are as critical anymore which is quite convenient when measuring on an IDDCA. The resulting MTF measurement is sparse, as we tailored which frequencies are generated by the CSIG so we know which frequencies to look for in the image acquired by the IRFPA. This is a global method which assumes identical pixels across the FPA like other existing MTF measurement methods relying on interference, random pattern and speckle [13–16]. However, this hypothesis is acceptable because T2SL are very promising in term of uniformity. The average MTF and spatial response can be obtained in a single measurement. As a bonus, the pixel size can be directly extracted from the measurements.This key parameter is essential for system designers as well as technologists.

The bench is made of a blackbody source, a pinhole, a collimator and the CSIG as described in Fig. 1. To project the intended frequencies on the FPA, the CSIG has to be illuminated in parallel beams [12], hence the need of a collimator. The size of the projected image of the blackbody on the CSIG has a filtering impact so a pinhole is there to ensure that the spatial frequencies have not been filtered out before even reaching the CSIG. The projected pattern of the CSIG is known by design [17] by specifying its period a_0 and its scaling factor η^2 which defines the projected frequencies. The raw image obtained by the FPA will be searched for amplitudes corresponding to the spatial frequencies contained in the projected pattern, which allows a 2D global MTF measurement as explained in details in [10].

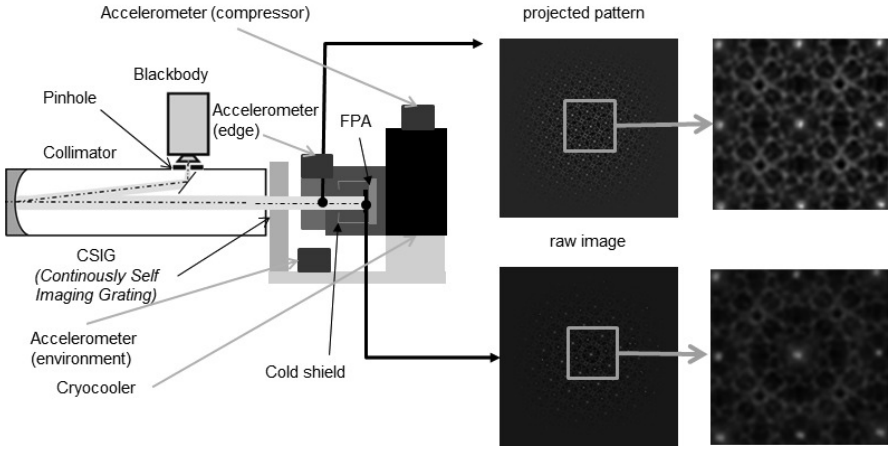

Fig. 1: Measurement bench using a CSIG. The collimated flux is projected by the CSIG following a pattern with known spatial frequencies. The raw image is recorded and processed in order to extract the pixel MTF.

The total measured MTF can be written as the product of the MTFs assigned for each contributor as illustrated on Fig. 2. We can first split the global MTF into 3 main contributors: the MTF of the CSIG, the MTF bound to the bench itself, the MTF due to the full IDDCA, with ν_x,ν_y being the spatial frequencies along x and y axes of the detector.

$$MTF_{total}(\nu_x, \nu_y) = MTF_{IDDCA}(\nu_x, \nu_y) \times MTF_{bench}(\nu_x, \nu_y) \times MTF_{CSIG}(\nu_x, \nu_y) \quad (1)$$

The CSIG generates a sparse MTF. Here it is made of 288 frequencies, which can be written as a sum of Dirac functions $\delta(\nu_{x_i}, \nu_{y_i})$ assigned with a weight c_i:

$$MTF_{CSIG}(\nu_x, \nu_y) = \sum_{i=1}^{288} c_i \delta(\nu_{x_i}, \nu_{y_i}) \quad (2)$$

The MTF_{bench} features a $\mathrm{MTF}_{pinhole}$ as the pinhole acts as a low pass filter defined by its diameter $\phi_{pinhole}$ and modelized by an Airy disk function A, and a $\mathrm{MTF}_{collimator}$ as well (whose focal length f will also define another cutoff frequency).

The MTF_{IDDCA} includes the $\mathrm{MTF}_{detector}$ we want to measure. Unfortunately, the $\mathrm{MTF}_{vibrations}$ is also part of the MTF_{IDDCA}: it is modelized by a 2D gaussian function G with 2 characteristic lengths δ_x and δ_y.

$$MTF_{IDDCA}(\nu_x, \nu_y) = MTF_{detector}(\nu_x, \nu_y) \times MTF_{vibrations}(\nu_x, \nu_y, \delta_x, \delta_y) \quad (3)$$

where:

$$MTF_{vibrations}(\nu_x, \nu_y, \delta_x, \delta_y) = G(\nu_x, \delta_x)G(\nu_y, \delta_y) = e^{\frac{(\pi\nu_x\delta_x)^2}{2}} \times e^{\frac{(\pi\nu_y\delta_y)^2}{2}} \quad (4)$$

Furthermore, we can see $\mathrm{MTF}_{detector}$ as a product of MTFs. First, the $\mathrm{MTF}_{idealpixel}$ (modelized by a 2D sinc and 2 characteristic lengths a_x^{pix} and a_y^{pix}) to describe the perfect behavior of an ideal rectangular pixel. The pixel is supposed to be rectangular, which allows the associated MTF as a 2D sinc function which cutoff frequency depends on a_x^{pix} and a_y^{pix} respectively. This assumption is critical and the reasons will be explained whenever this hypothesis is needed throughout the paper. Second, a MTF_{tech} (modelized by a 2D gaussian and parameters d_x and d_y), that describes effects such as electronic diffusion that alter the $\mathrm{MTF}_{detector}$. The MTF_{tech} assumes that every effect altering the $\mathrm{MTF}_{idealpixel}$ can be encompassed and described by a single MTF with independent parameters d_x and d_y.

$$MTF_{detector}(\nu_x, \nu_y) = MTF_{idealpixel}(\nu_x, \nu_y) \times MTF_{tech}(\nu_x, \nu_y) \quad (5)$$

with:

$$MTF_{idealpixel}(\nu_x, \nu_x) = sinc(\nu_x a_x^{pix}) \times sinc(\nu_x a_y^{pix}) \quad (6)$$

and:

$$MTF_{tech}(\nu_x, \nu_y) = G(\nu_x, d_x)G(\nu_y, d_y) \quad (7)$$

An accelerometer is put on the cryocooler compressor as we can assume it is the source of the vibrations and two more are put on the bench and on the edge of the cooler assembly (see Fig. 1). Accelerometer measurements will be commented in part 3.

Optics EXPRESS

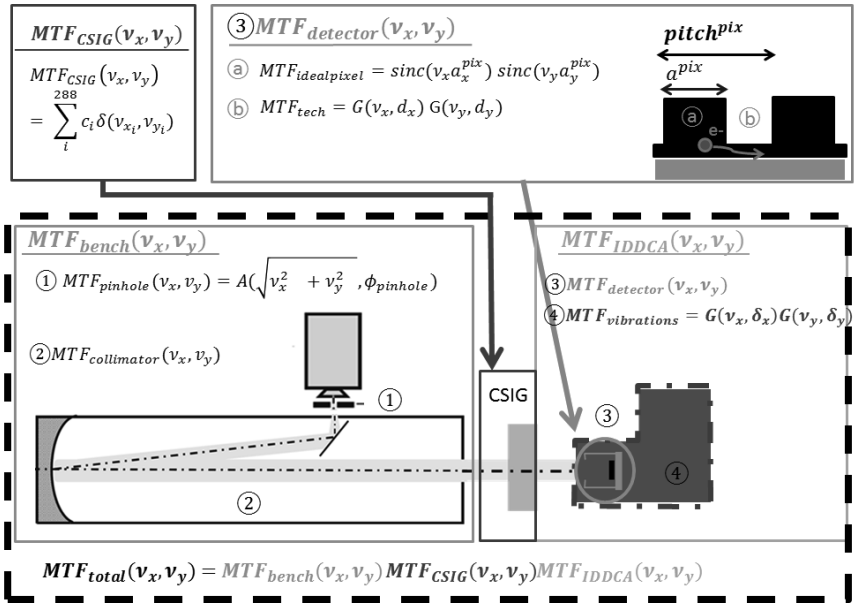

Fig. 2: Measured MTF breakdown. The total MTF can be divided into 3 main blocks: the MTF_{CSIG}, the MTF_{bench} and the MTF_{IDDCA}. The MTF_{bench} can be split into $\mathrm{MTF}_{pinhole}$ and $\mathrm{MTF}_{collimator}$. The MTF_{IDDCA} can be divided in $\mathrm{MTF}_{vibration}$ and $\mathrm{MTF}_{detector}$. d_x, d_y, δ_x, δ_y and $\phi_{pinhole}$ are parameters described in the text.

2.2. Design of the bench

Measurements were made using a Smaract mechanical stage, a CI Systems collimator (f=762mm) and a 1473K blackbody. The IDDCA tested here is a MWIR 320x256 T2SL FPA with 30µm pitch, made by IRnova. The FPA is a InAs/GaSb MWIR type-II superlattice operating at 80K. Integration time t_i has been set to 6ms to ensure the measured pattern is well contrasted. The number of images has been set to 300 (with a framerate of 60Hz) in order to have enough images to improve the signal to noise ratio while maintaining a short measurement time.

The whole purpose of the bench designing phase is to ensure that $\mathrm{MTF}_{detector}$ is far more significant compared to $\mathrm{MTF}_{pinhole}$, $\mathrm{MTF}_{collimator}$ and, if possible, $\mathrm{MTF}_{vibration}$ (respectively labeled as 1, 3, 4 and 2 in Fig. 2). As such, the collimator has been chosen so that $MTF_{collimator}(\nu)$ is close to 1.

Three points demand special attention to make sure the $\mathrm{MTF}_{detector}$ is the main contributor of the MTF we will measure.

- First, the choice of the CSIG itself is important as it defines by its period a_0 and scaling factor η^2 the maximum frequency excited by the grating :

$$\nu_{max} = \frac{2\eta}{a_0} \tag{8}$$

The CSIG we chose is an amplitude grating, without antireflection coating. It has a η^2 of 650 (24 orders) and a period of 1mm, which gives $\nu_{max} = 51mm^{-1}$.

- Second, we have to mitigate spatial filtering effect of the pinhole of diameter $\phi_{pinhole}$ by having its cutoff frequency as far as possible. This cutoff frequency is defined by the diameter of

its image ϕ' on the FPA :

$$\nu_{pinhole} = \frac{1.22}{\phi'} \tag{9}$$

where:

$$\phi' = \phi_{pinhole}\frac{d}{f} \tag{10}$$

with f the focal length of the collimator and d the CSIG-FPA distance. As the diameter of the pinhole diminishes, the cutoff frequency increases, but this also results in a reduced incoming flux on the CSIG , which does not favor the signal-to-noise ratio. We took a 500µm pinhole and ensured that the FPA still could detect the pattern. Assuming that $d < 30mm$ and knowing that f=762mm, we have $\nu_{pinhole}$>$62mm^{-1}$. The pinhole is guaranteed not to be the limiting factor in this setup.

- Last, the cryocooler creates and transmits vibrations to the FPA. Unfortunately, the signature of such vibrations is similar to technological effects and will have to be evaluated a posteriori (see Results and discussion).

Caution is needed on another point. On the one hand, the CSIG has to excite and project on the FPA frequencies beyond the cutoff frequency of the pixel. We chose a CSIG whose max frequency is as high as ν_{max} =51 mm^{-1}, guaranteeing to be able to measure a pixel size greater than $a_{min}^{pix} = \frac{1}{\nu_{max}}$ =20 µm. This minimum size hypothesis is enabled precisely because we assume that the pixel is rectangular (indeed, the cutoff frequency is not guaranteed to be equal to the pixel size outside this hypothesis). On the other hand, the FPA has to properly sample the projected pattern and the FPA cannot sample properly frequencies beyond its Nyquist frequency of $16,67mm^{-1}$ ($=\frac{1}{2pitch^{pix}}$) under normal conditions.To meet both requirements, we chose to oversample the image by microscanning, in order to push the Nyquist frequency of the equivalent pitch beyond ν_{max}. A 5x oversampling with a 6µm step has been chosen, increasing the image resolution thus extending the Nyquist frequency to 83,3 mm^{-1}.

Different microscanning patterns have been tested. The spiral pattern as shown on the left hand side of Fig. 3 was most faithfully reproduced by the mechanical stage, as probably this movement pattern helps mitigate the hysteris observed on other patterns.

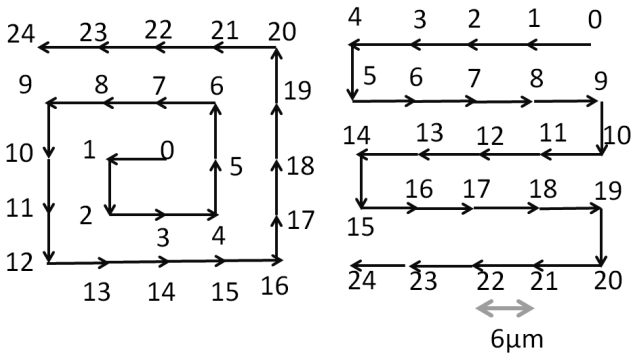

Fig. 3: Patterns used for oversampling on this bench, the left pattern being reproduced more faithfully by the mechanical stage.

2.3. Results

The measured MTF is displayed in Fig.4. The MTF is bi-dimensional. However, because we chose to represent the MTF as a function of $\nu = \sqrt{\nu_x^2 + \nu_y^2}$, dispersion is expected. Indeed the diagonal length will also act as a cutoff frequency. That is to say the border length (corresponding to a cutoff frequency) will be different based on whether we look along x (or y) direction or the diagonal (x+y) direction (since we assumed that the pixel is rectangular). For this reason, models along x,y and x+y direction should be drawn. Since $\mathrm{MTF}_{vibration}$ and $\mathrm{MTF}_{diffusion}$ have the same gaussian signature and $\mathrm{MTF}_{collimator}(\nu)$ being close to 1, comparison is made with the following model simplified from Eq. (1) with G being the gaussian function which comprises here vibration and technological effects (see Fig. 2) :

$$MTF_{total}(\nu_x, \nu_y) = MTF_{pixel}(\nu_x, \nu_y)G(\nu, \delta_x)G(\nu, \delta_y) \tag{11}$$

where δ_x and δ_y are 2 adjustable parameters. Best agreement with the data is found for δ_x=δ_y = 10µm. Gaussian functions do not have zeros, so only two contributions may cancel the MTF : the pixel MTF and the pinhole MTF. The pinhole diameter has been chosen so that the cutoff is much further than the pixel cutoff so that the first cancellation of the measured MTF is due to the pixel MTF. It is important to note that the first zero of the pixel MTF is at $\nu = \frac{1}{a^{pix}}$ (again, the formula is valid because the pixel is supposed to be rectangular). It also happens to be $\nu = \frac{1}{pitch^{pix}}$ only when the fill factor (which we define as the ratio between the actual pixel size and the pitch) of the FPA is equal to 1. It is worth noting that the pixel size is already extractable regardless of the other contributions of the global MTF. However, it may be difficult to estimate the first zero of the experimental measurement of the modulus of the MTF. It can be more reliable to look for a change of sign than just a zero to determine the pixel size. Therefore the argument of the IDDCA MTF is displayed on Figure 4 and we estimate $\nu_{pixel} = 39mm^{-1}$ that is to say a_x^{pix}=a_y^{pix}=26µm for a 30 µm pitch. The 26µm square pixel size matches with the expected value. It means that the bench can be used as a non destructive technique to estimate the pixel size of an operational FPA.

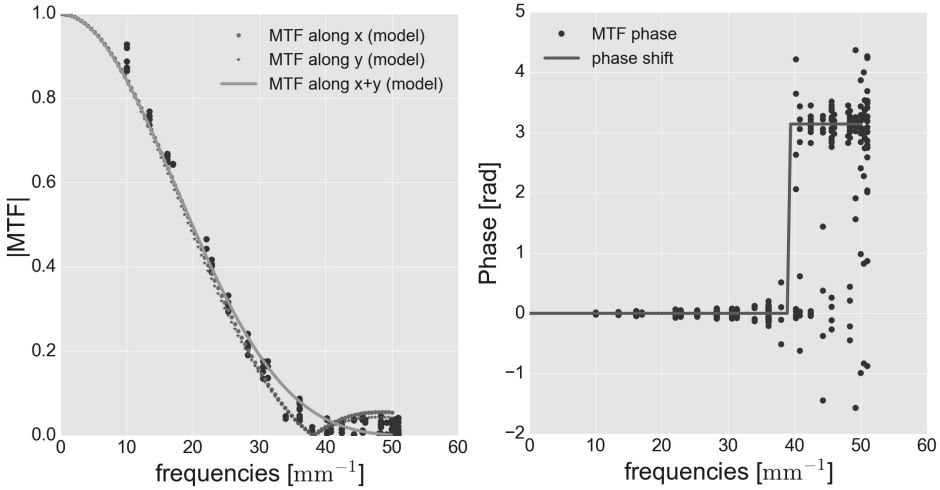

Fig. 4: IDDCA MTF measurement : on the left, the modulus of the IDDCA MTF as a function of spatial frequency; on the right, the argument of the IDDCA MTF as a function of spatial frequency. The phase shift drawn is only a guide for the eye.

3. Discriminating technological effects and vibrations

Up to now, we measured MTF_{IDDCA}. We still need to distinguish $\mathrm{MTF}_{vibration}$ from MTF_{tech}. Vibrations whose frequency is lower than $\nu = \frac{1}{2t_i} = 83$ Hz can be seen as translations along x and y axes from an image to another. Because the frequencies excited by the CSIG are known, it is possible to view these same vibrations as phase shifts in the Fourier domain. Namely, be Img a given image, $TF(Img)$ its Fourier decomposition, x_0 and y_0 the translation in x and y axes, we have:

$$TF(Img(x - x_0, y - y_0)) = TF(Img)e^{-2i\pi(\nu_x x_0 + \nu_y y_0)} \tag{12}$$

By making use of the Fourier decomposition on each of the 300 images and fitting the exponential in Eq. (12), it is possible to extract a (x_0,y_0) translation for each position and estimate the typical vibrations amplitudes on x and y axes.

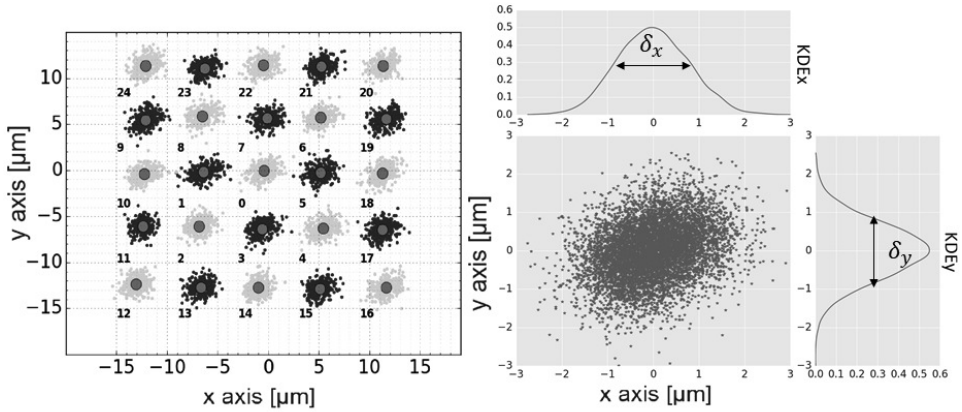

Fig. 5: On the left : vibrations estimated on each of the 25 positions taken by the CSIG (marked with a number). The bigger dot represents the average position of the 300 averaged images. On the right, the measurements after merging the average positions. Colors were only meant to distinguish acquisitions on different positions.

As shown in Fig. 5, we estimate the vibration amplitude as the Full Width Half Maximum (FWHM) using Kernel Density estimations. An average amplitude δ_x = 1.2 µm is found in the image on the horizontal axis and 1.2 µm amplitude δ_y on the vertical axis. The same pattern is found on each position, which is coherent with the fact that vibrations affects the whole FPA.

3.1. Vibrations frequency range and their effects

Vibrations induce a spread on the position occupied by the FPA. Therefore they will affect the MTF measurement depending on the frequencies they contain. We will assume for clarity purpose that the vibration is a 1D sinusoid as depicted in Fig. 6 but what is explained still remains true in 2D. Four cases can be highlighted depending on the vibration frequency f_{vib}:

- Case 0 is the ideal case where vibrations are non existent. Every single image is sharp and there is little dispersion in the returned position from an image to another.

- Case 1 :$f_{vib} \ll \frac{1}{2t_i}$. FPA barely moves during t_i so single images are sharp but shifts will appear as averaging requires multiple images. Measuring a faithful MTF is achievable provided

data processing (Shift-and-adding is a remedy in this case).

- Case 2 : $f_{vib} \gg \frac{1}{2t_i}$, the FPA on contrary describes the full periodic vibration pattern during the integration time. Single images are blurry but the dispersion in the returned position of each blurry image will be low, misleading into thinking that there is less vibrations than there actually is. The MTF is possibly distorted. Additional efforts are required to determine if the amplitude of the vibration is high enough to strongly distort the MTF.

- Case 3 is when f_{vib} can compare to $\frac{1}{2t_i}$. The drawbacks of the two previous cases overlap. Some images are sharp, some are not. One can consider sorting out and using only the sharpest images (a.k.a. Lucky imaging) to return in case 1 but in our case, we will look for an upper bound of the impact on the MTF.

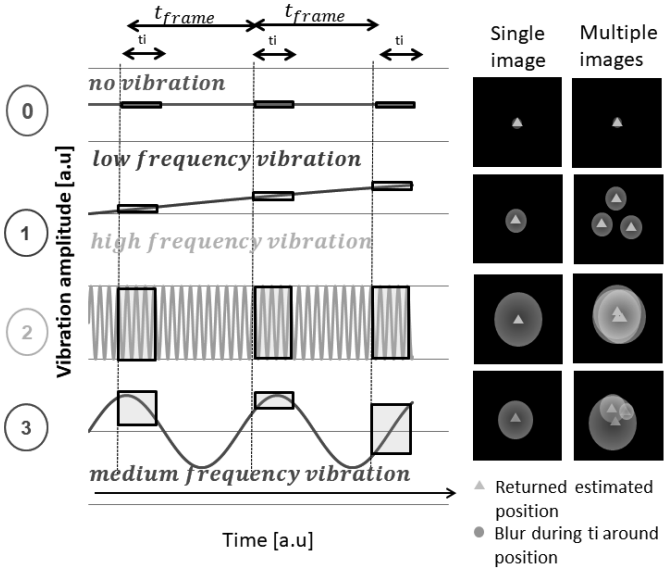

Fig. 6: Comparison of the vibrations period with the integration time t_i. t_{frame} (16.6 ms) represents the time interval between 2 images. From top to bottom: 0) no vibration 1) low frequency vibration 2) high frequency vibration 3) medium frequency vibration. For each case, the periodic vibration is compared to t_i and t_{frame} on the left ; on the right, the resulting effect on a single image and upon acquiring multiple images is displayed.

3.2. Accelerometer measurements

Given the importance of which vibrations are present in our analysis, we decided to implement accelerometer measurements using 3 crossbow CXL04GP3 accelerometers (200Hz bandwidth).

The first one is put on the compressor of the cryocooler as we assume it is the source of vibration. Besides, the second one is put on the measurement bench (on the breadboard), in order to verify that the lab environment does not transmit other vibrations. The last one is put near the edge of the IDDCA, (geographically) close to the FPA position. We ensured the bench does not receive any vibration from the environment before starting measurements by comparing the data acquired from the accelerometer bound to the cryocooler and the one on the bench. On the

breadboard data, we can see a 50Hz peak that does not appear on the compressor data. This 50Hz on z axis stems from the fan air cooling system imbedded in the power supplies operating nearby the bench. The fans induced a 3D 50Hz vibration that has been mitigated in x and y axes because of the mass of the breadboard. Moreover, data from the edge of the IDDCA proves that there is no propagation in the outer mechanical structure of the IDDCA (see Fig. 7).

The data shows that there is no low frequency vibration but there is a significant peak at 31Hz. This frequency is neither far higher nor far lower than $\frac{1}{2ti}$: we are typically in case 3. This peak shifts as we change the cryocooler operating temperature, meaning that this particular 31Hz frequency is due to this cryocooler operating at 80K.

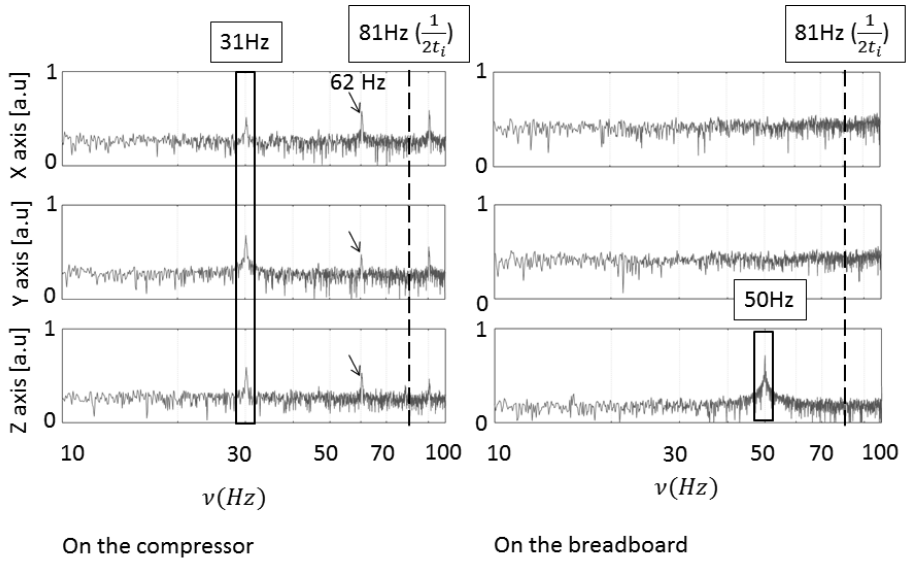

Fig. 7: Vibration spectrum measured on the compressor (left) and on the measurement bench (breadboard, right). X represents the optical axis, Y, Z the FPA plane. On the compressor data, we can see a 31Hz peak and its harmonics (notably one at 62Hz). The bandwidth due to integration time (81Hz) is displayed as well. On the breadboard data, we can see a 50Hz peak that does not appear on the compressor data. We can conclude that the IDDCA is well isolated from the lab environment.

3.2.1. Evaluation of the 31Hz frequency vibration on the MTF

We need to evaluate in our configuration the impact of the vibration at 31Hz on the MTF data. For the sake of clarity, the FPA position can be modelized as a 1D sinusoid function of time pos(t), but this remains true in 2D (with 2 separate 1D sinusoids).

$$pos(t) = Asin(2\pi \times t \times f_{vib}) \tag{13}$$

where t is the time, f_{vib} the vibration frequency, A the half amplitude of the sinusoid. Maximum displacement d_{max} is then given by finding the maximum of pos(t) derivative and multiplying by t_i:

$$d_{max} = 2\pi A \times f_{vib} \times t_i \tag{14}$$

d_{max} represents the upper boundary of the shift that can occur during t_i. As it represents the worst case scenario in term of blur within an image, we will use Eq. (14) to evaluate the worst

impact on the MTF this 31Hz vibration can have. While the amplitude of those vibrations on the FPA cannot be retrieved with the sole accelerometer measurement, it is still possible to have a good estimation of the upper boundary of the blur. As we noted in the right panel of Fig. 5, we estimated δ_x, δ_y=1.2 µm amplitude for the vibration, so this is why we can safely assume that 1.2 µm represents a good estimation of A. Applied with A=1.2 µm, t_i=6ms and f_{vib}=31Hz we find d_{max}=1.4 µm on both axes here.

Let's suppose that the FPA can move up to 1.4 µm during t_i within a single image (case 3). The impact of the shift within the elementary image can be seen as convoluting the pixel with a 1.4 µm wide window (or multiplying by a sinc in Fourier space). Considering MTF_{vibpix} is the MTF of the vibrating pixel, MTF_{pixel} the MTF due to the pixel only and MTF_{vib} the MTF due to vibration, we have in Fourier space:

$$MTF_{vibpix}(\nu_x) = MTF_{pixel}(\nu_x) \times MTF_{vib}(\nu_x) = MTF_{pixel}(\nu_x) \times sinc(\nu_x 1.4\mu m) \quad (15)$$

At Nyquist frequency ($\nu_{Nyq} = \frac{1}{2pitch^{pix}}$), with $pitch^{pix}$=30 µm we have $MTF_{vib}(\nu_{Nyq}) = 0.997$, which is very close to 1.

Let's assume the other extreme scenario that consecutive images can shift by 2.4 µm ($2\times A$) (case 1). This 2.4 µm shift is totally similar to a line of sight stabilization residual in an electro-optical system. This can be modelized as :

$$MTF_{stab}(\nu_x) = e^{-2(\pi\sigma_{stab}\nu_x)^2} \quad (16)$$

with σ_{stab}=2.4µm.

Numerical application at ν_{Nyq} yields $MTF_{stab}(\nu_x) = 0.97$. Compared to the pixel filtering effect at Nyquist frequency ($sinc(\nu_{Nyq})$=0.72), we see that such a shift will not have sizeable influence on the MTF.

We can conclude that the 31Hz vibration has been evidenced as non harmful on our MTF measurement. Only low and medium frequency vibrations have been studied thus far (cases 1 and 3 in Fig. 6). The high frequency vibrations (case 2) are integrated during t_i and may have significant effect on the MTF. Since the accelerometer is not perfectly adapted to detect the high frequencies due to its bandwidth (200Hz), this case 2 warrants dedicated studies and measurements that are presented hereafter.

3.3. Low integration time complementary measurements

So far, we know there is a 31Hz vibration which does not strongly affect the MTF. We need now to ensure that no high frequency vibration has been integrated during t_i. Our approach is to estimate the δ_x, δ_y parameters as a function of t_i. We can see δ_x, δ_y as the standard deviation of the position on the FPA during t_i. It is important to remember that the SNR also decreases as t_i is shorter. As demonstrated in [18] for a backgroundless scene (but can be extended to our case as adding a constant background does not alter the result), δ_x and δ_y vary as $\frac{1}{\sqrt{t_i}}$ when limited by photon noise. Our bench is limited by photon noise, as the background signal (the blackbody) is predominant and has to be subtracted before extracting the MTF. Should there be any high frequency vibrations, they should affect δ_x and δ_y estimations, thus no longer making them as function of $\frac{1}{\sqrt{t_i}}$ alone.

For that purpose, we estimated the vibration amplitude δ_x and δ_y while changing the integration time, ranging from 16ms to 0.2ms, thus increasing the bandwidth of our measurement. We did not make any modification on the MTF measurement bench, meaning that the setup has not changed in terms of vibrations. Here, there is no microscanning as we are not interested in measuring the MTF but only in how well the positions are evaluated. This is equivalent to only measuring 1 of the 25 positions in the previous paragraph, and this time we take 900 images instead of 300. The

vibration amplitudes δ_x and δ_y are now a function of t_i and results are found in Fig 8. Both have been fitted with a function proportional to $F(t) = \frac{1}{\sqrt{t_i}}$.

Since there is good agreement with the experimental data we can tell that there are no high frequency vibrations impacting the MTF bench at the time of measurement. By combining accelerometer measurements and low t_i measurements we showed that the reported measurements are void of vibrations effects whose frequencies are up to $\frac{1}{2\times 0.2ms}$=2.5 kHz.

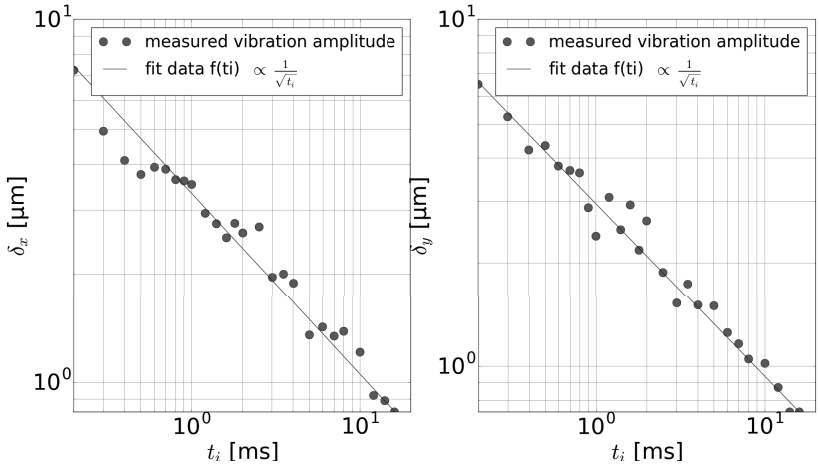

Fig. 8: Vibration amplitude estimation as a function of integration time on x (left) and y axes (right).

4. Conclusion

In this work, we report on a MTF measurement bench using the diffraction properties of a Continuously Self Imaging Grating (CSIG). This bench is used for the MTF measurement of a type-II superlattice infrared detector in operational packaging. The bench does not require high-end optics to project the pattern with known spatial frequencies. It also significantly lowers alignment and focusing requirements, a convenience especially when the detector needs to be cooled. At last, this study allows to tell vibrations effects and technological contribution apart, making the bench a strong contender for MTF measurements on infrared FPA. The IDDCA configuration of the characterized 30µm pitch type-II InAs/GaSb superlattice FPA required to lead dedicated additional vibrations studies along the MTF measurement. Finally, the CSIG bench allows to determine the pixel size in the same process as well. In the particular case of the T2SL FPA, a 26µm pixel size has been measured and is relevant with the expected value, giving access to a key detector parameter.

Funding

Labex FOCUS (ANR-11-LABX-0013).

Acknowledgments

We would like to acknowledge the fruitful discussions with IRnova. We also thank the Labex Focus for its financial support.